Wear Mechanisms of Carbon-Based Refractory Materials in Silicomanganese Tap Holes—Part I: Equilibrium Calculations and Slag and Refractory Characterization

J.D. STEENKAMP, P.C. PISTORIUS, and M. TANGSTAD

Silicomanganese (SiMn) as an alloy supplies silicon and manganese to the steelmaking industry. It is produced through carbothermic reduction in a submerged arc furnace. The slag and metal are typically tapped through a single-level tap hole at 50 K (50 °C) below the process temperature of 1873 K to 1923 K (1600 °C to 1650 °C). In one tapblock refractory design configuration, the tap hole is installed as a carbon tapblock and rebuilt during the life of the lining using carbon-based cold ramming paste. The carbon tapblock lasts for a number of years and ramming paste only for months. The purpose of the study presented here was to determine to what extent chemical reactions between carbon-based refractory and slag or metal in the tap hole of a SiMn furnace can contribute to wear of tap-hole refractory. The results of the study are reported in two parts. In Part I, the results of thermodynamic calculations of the potential for chemical reaction between carbon-based refractory material and slag or metal are reported. The results were tested experimentally using pure graphite and synthetic SiMn slag (produced from pure oxides). The paper also reports the composition, microstructure, and phases of industrial SiMn slag, and commercially available carbon block and cold ramming paste refractory materials. These compositions were used in predicted equilibria of refractory–slag reactions. Thermodynamic calculations suggest that reaction between SiMn slag and carbon-based tap-hole refractory is possible, and experiments with nominally pure materials support this. However, practical refractory materials are by no means pure materials, and contain secondary phases and porosity which can be expected to affect reaction with slag. Such reactions are examined in Part II.

I. INTRODUCTION

SILICOMANGANESE (SiMn) is one of the alloys commercially available for the addition of manganese to steel during the steelmaking process.[1] SiMn is produced by reducing oxides containing manganese and silicon with carbonaceous reductant in a submerged arc furnace (SAF) at typical process temperatures around 1873 K to 1923 K (1600 °C to 1650 °C)[2,3] and tapping temperature 50 K (−223 °C) lower.[1] Typical compositions of alloy and slag are given in Tables I and II.[1]

The tap hole is one of the high-wear areas in SAFs producing SiMn.[5] Two types of carbon-based materials are typically installed as tap-hole refractory in these furnaces: carbon block and cold ramming paste.[6,7]

Carbon bricks or blocks are produced from aggregate (electrically or gas calcined anthracite, calcined coal, petroleum coke, carbon black, artificial graphite, or combinations of these) and binder (petroleum pitch or coal tar). For carbon blocks, the raw materials are mixed, shaped, and baked at 1073 K to 1673 K (800 °C to 1400 °C) to carbonize the binder. To produce graphite blocks, an additional graphitizing step at 3273 K (3000 °C) is required.[8–10] To reduce the poros-ity of carbon bricks or blocks, the fired material is impregnated with binder material and refired.[10] To strengthen the bond matrix, generate microporosity, or improve wear resistance properties, metallic Si, SiC, Al_2O_3, Ti, or TiO_2 is added.[9,10]

Cold ramming paste typically consists of aggregate (electrically calcined anthracite) and binder (coal tar pitch). The binder carbonizes at 773 K (500 °C) but should be baked at 1223 K (950 °C) after installation.[11] Electrically calcined anthracite [produced at temperatures of 1473 K to 3273 K (1200 °C to 3000 °C)] contains 30 to 40 pct graphite; gas calcined anthracite [produced at a lower temperature of 1473 K (1200 °C)] does not contain graphite.[11]

In this work, possible reactions between such carbon-based refractories and furnace fluids (slag and metal) were studied. Although slag, metal, and carbon might approach chemical equilibrium inside the furnace at

J.D. STEENKAMP, formerly Graduate Student with the Department of Materials Science and Metallurgical Engineering, University of Pretoria, Pretoria, South Africa, is now Chief Engineer with the Pyrometallurgy Division, Mintek, Randburg, South Africa, P.C. PISTORIUS, POSCO Professor, is with the Department of Materials Science and Engineering, Carnegie Mellon University, Pittsburgh, PA. Contact e-mail: pistorius@cmu.edu and also Extraordinary Professor with the Department of Materials Science and Metallurgical Engineering, University of Pretoria. M. TANGSTAD, Professor, is with the Department of Materials Science and Engineering, Norwegian University of Science and Technology (NTNU), Trondheim, Norway.

Manuscript submitted November 17, 2014.
Article published online January 6, 2015.

process temperatures of 1923 K (1650 °C),[1] industrial examples of slag and metal attack of carbon refractories were reported[12] implying that the slag, metal, and carbon refractories were not at chemical equilibrium. The purpose of the study presented here was to determine to what extent chemical reactions between carbon-based refractory and slag or metal in the tap hole of a SiMn furnace can contribute to wear of tap-hole refractory.

The results of the study are reported in two parts:

1. *Part I* presents the results of thermodynamic calculations of the potential for chemical reaction between carbon-based refractory material and slag or metal (using published chemical compositions as inputs). The results of the thermodynamic calculations were tested experimentally using pure graphite and synthetic SiMn slag (produced from pure oxides). The paper also reports the composition, microstructure, and phases of industrial SiMn slag, and commercially available carbon block and cold ramming paste refractory materials. These compositions were used in predicted equilibria of refractory–slag reactions.
2. *Part II* presents the results of experimental studies conducted to test the potential for chemical reaction between synthetic SiMn slag and commercially available carbon-based refractory materials.

II. EQUILIBRIUM CALCULATIONS

Equilibria between slag and metal and carbon (and possible product gas) were calculated (for different temperatures) using FactSage 6.4[13] (FToxid, FactPS, and FSstel databases). For calculations involving slag only, a small mass of argon (10^{-7} times the slag mass) was included in the calculation, to allow formation of a small fraction of trivalent manganese in the slag, and selecting as possible product phases the liquid slag solution (SLAGA, considering possible two-phase immiscibility), spinel and monoxide solution (ASpinel and AMonoxide), all other solution phases, pure solids and pure liquids, and an ideal-gas mixture.

Possible reactions between slag or metal and refractory were investigated by allowing equal masses of slag

Table I. Typical Composition of Tapped SiMn Alloy (Mass Percent)[1]

	pctMn	pctSi	pctC	pctFe
Typical[1]	68	20	2	10
Elkem Marietta[4]	65.9	19.1	1.38	
Samancor M12[4]	67.7	17.5	1.18	16.0
Samancor M13[4]	65.5	17.8	1.15	15.5

Table II. Compositions of Tapped SiMn Slags (Mass Percent): Typical Slags,[1] and Industrial and Synthetic Slags Used in This Work (Averages, with Standard Deviation in Parenthesis Where Applicable)

	pctMnO	pctSiO_2	pctAl_2O_3	pctCaO	pctMgO	pctFeO
Typical	9	45	16	21	9	0
Industrial	7.5 (0.2)	45.3 (0.5)	16.5 (0.1)	23.5 (0.4)	7.1 (0.02)	0.1 (0.1)
Synthetic-ICP	11.3 (0.3)	44.3 (0.2)	15.5 (0.1)	23.8 (0.1)	5.2 (0.1)	
Synthetic-EDS	10 (0.2)	47 (0.3)	16 (0.1)	22 (0.2)	5 (0.1)	

For synthetic slag, results from both bulk (ICP) analysis and EDS microanalysis are reported.

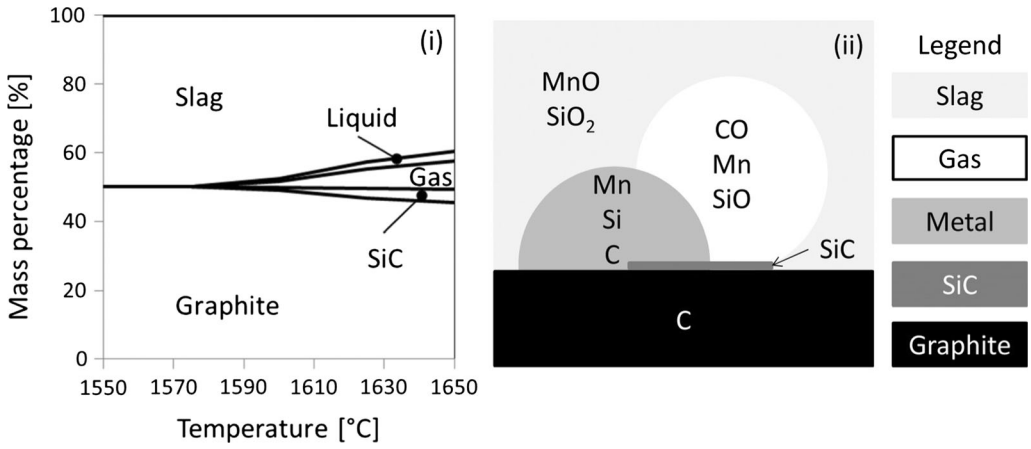

Fig. 1—(*i*) Equilibrium phase composition as a function of temperature, when reacting graphite (representing refractory) with an equal mass of silicomanganese slag (with typical composition as in Table II). (*ii*) Cartoon of potential equilibrium phases and participating components per phase when slag equilibrates with graphite.

(or metal) and refractory to equilibrate, considering temperatures from 1823 K to 1923 K (1550 °C t o 1650 °C), and the typical compositions listed in Tables I and II.

The calculated liquidus temperature of the slag is 1508 K (1235 °C) with anorthite (CAS_2) as the primary phase. Equilibrium phases for mixtures of slag and carbon are shown in Figure 1(i); corresponding equilib-rium slag, metal, and gas compositions are given in Tables III, IV, and V.

Activity data for metal components were calculated with FactSage (FSstel database), and also by utilizing the interaction parameters of Li and Morris;[14] equilib-rium constants were calculated with FactSage, using the reference states listed in Table VI; calculated values are given in Tables VII (slag) and VIII (metal).

Based on these calculations, the slag can react with graphite to form solid SiC, liquid metal, and gas (Figure 1), for temperatures of 1873 K (1600 °C) and higher. MnO is reduced to form Mn in liquid metal (Table IV) and in gas (Table V); SiO_2 is reduced to form solid SiC, Si dissolved in liquid metal (Table IV), and SiO in the gas (Table V). Carbon would dissolve in the Mn-Si-C product (Table IV).

Reaction of tapped silicomanganese (with the com-position listed in Table I) with carbon is also predicted to be possible: the activity of dissolved carbon is smaller than 1 (Table VIII), and hence the metal can dissolve more carbon. Carbon saturation of Mn-Si-Fe-C alloys involves equilibrium with graphite for lower-Si alloys, and with silicon carbide in higher-Si alloys. As illus-trated in Figure 2, dual saturation (with graphite and silicon carbide) occurs at [pctSi]≈16.5 pct at 1873 K (1600 °C), for Mn:Fe ratios in the range encountered in industrial alloys. (The saturation diagram reported by Olsen *et al.*[1] indicates somewhat higher carbon solu-bility, but similar silicon contents at dual saturation.) The ''typical'' metal composition in Table I is calculated to be supersaturated with silicon carbide; this may simply be a result of low precision of the reported composition (rounding). If this composition is accurate, equilibration of such metal with graphite would involve dissolution of carbon and precipitation of silicon car-bide, causing the metal composition to change as indicated in Figure 2. All the reported silicomanganese compositions (Table I) have silicon contents higher than dual saturation (Figure 2); any of these metal compo-sitions would tend to dissolve pure carbon.

If simultaneous contact of silicomanganese and slag with carbon were to occur, the tendency for reaction would depend on the activities of dissolved species in the metal. Table IX summarizes the predicted possibility of

Table III. Chemical Composition of Slag (Mass Percent) After Equilibration with Graphite at 1 Atm Total Pressure

T [K (°C)]	MnO	SiO_2	Al_2O_3	CaO	MgO
1823 K (1550 °C)	9.0	45.0	16.0	21.0	9.0
1848 K (1575 °C)	9.0	45.0	16.0	21.0	9.0
1873 K (1600 °C)	7.2	44.4	16.8	22.1	9.5
1898 K (1625 °C)	4.9	41.3	18.7	24.6	10.5
1923 K (1650 °C)	3.3	38.7	20.2	26.5	11.3

Table IV. Chemical Composition of the Metal Phase (Mass Percent) After Equilibration of Slag with Graphite at 1 Atm Total Pressure

T [K (°C)]	C	Mn	Si
1873 K (1600 °C)	2.0	70.9	18.1
1898 K (1625 °C)	2.1	70.7	18.3
1923 K (1650 °C)	2.1	70.4	18.6

Table V. Chemical Composition of the Gas Phase (Volume Percent) After Equilibration of Slag with Graphite at 1 Atm Total Pressure

T [K (°C)]	CO	Mg	SiO	Mn
1873 K (1600 °C)	98.0	0.1	0.7	1.2
1898 K (1625 °C)	97.6	0.2	0.8	1.5
1923 K (1650 °C)	97.0	0.4	0.8	1.8

Table VI. Standard Reference States Applied in the Calculation of Equilibrium Constants of Relevant Chemical Reactions

Component	MnO	SiO_2	C	Mn	Si	CO	SiC
Reference state	pure liquid	pure liquid	pure graphite	pure liquid	pure liquid	gas (1 atm)	pure cubic

Table VII. Activity of Slag Components (Calculated with FactSage 6.4) for Typical Slag Analysis in Table II; Reference States as in Table VI

T [K (°C)]	SiO_2	MnO	Al_2O_3	CaO	MgO
1823 K (1550 °C)	0.21	0.021	0.0066	0.00052	0.0094
1848 K (1575 °C)	0.21	0.022	0.0066	0.00059	0.0096
1873 K (1600 °C)	0.21	0.023	0.0066	0.00067	0.0097
1898 K (1625 °C)	0.21	0.025	0.0066	0.00075	0.0099
1923 K (1650 °C)	0.21	0.026	0.0066	0.00085	0.0100

Table VIII. Activity of Metal Components (Calculated with FactSage 6.4 and the Interaction Parameters of Li and Morris), for Typical Metal Composition in Table I; Reference States as in Table VI

	FactSage			Li and Morris		
T [K (°C)]	Mn	Si	C	Mn	Si	C
1823 K (1550 °C)	0.20	0.042	0.76	0.17	0.031	0.69
1848 K (1575 °C)	0.20	0.046	0.77	0.18	0.032	0.63
1873 K (1600 °C)	0.20	0.051	0.77	0.18	0.033	0.58
1898 K (1625 °C)	0.20	0.056	0.78	0.18	0.034	0.53
1923 K (1650 °C)	0.19	0.061	0.79	0.18	0.035	0.49

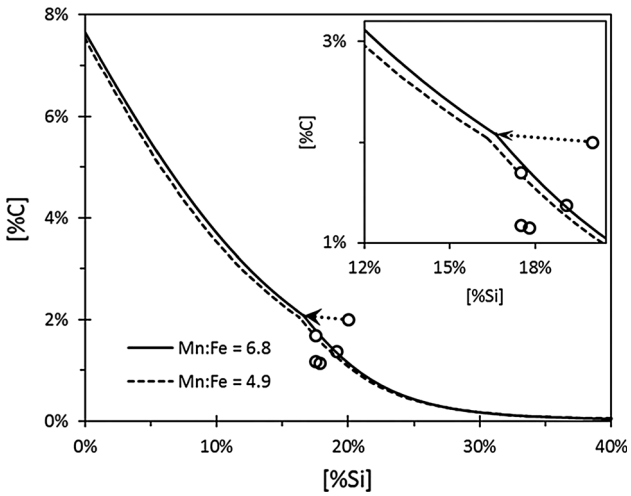

Fig. 2—Carbon solubility in Mn-Fe-Si-C alloys with two Mn:Fe mass ratios at 1873 K (1600 °C), calculated with FactSage 6.4 (FSstel database); compositions given as mass percentages. For sili-con contents below the inflection in the curve, the stable solid phase at saturation is graphite; SiC is the stable phase at saturation for higher silicon contents. The symbols show reported silicomanganese compositions (Table I); for one of these, the predicted change in composition upon equilibration with graphite is shown by the arrow, terminating at dual saturation with graphite and SiC (inset is an en-larged view).

reaction, using the slag-species activities from Table - VII, and the two sets of metal-species activities from Table VIII. The tendency to react is summarized as the ratio (Q/K), where Q (the reaction quotient) is the actual ratio of activities of products to reactants, and K is the equilibrium constant; if $Q/K < 1$, the forward reaction is possible.

As also mentioned earlier, Table IX indicates that reactions which may lead to chemical wear of carbon-based tap holes are the reduction of SiO_2 to produce SiC or alloyed Si, reduction of MnO to alloyed Mn, and the dissolution of carbon in metal up to the point of dual saturation. Depending on the model applied in calcu-lating the activities of the metal components, the production of SiC, alloyed Si, and alloyed Mn should be possible at 1873 K (1600 °C)[14] or SiC and alloyed Mn should form, but not alloyed Si.[13] In addition, the metal —formed either by the slag reactions or present as tapped metal—would be saturated in SiC but not in C, and would therefore tend to dissolve carbon and further produce SiC to reduce the Si content until dual saturation was reached. It is predicted that none of the reactions would be possible at 1823 K (1550 °C), and at 1923 K (1650 °C) all reactions would occur. As reported later in this paper, the possibility of reaction at 1923 K (1650 °C) was confirmed with laboratory tests.

III. COMPOSITION AND MICROSTRUCTURE: INDUSTRIAL SLAG AND CARBON REFRACTORY

A. *Sampling and Analysis*

The equilibrium calculations reported in the previous section indicate that reaction of carbon with both metal and slag may contribute to chemical wear of carbon-based refractory. A likely complicating factor is that practical carbon refractory is not pure carbon; the composition and microstructure of the refractory are expected to affect the rate and extent of reaction with metal and slag. In this section, the microstructure, phase composition, and chemical composition of two types of carbon-based refractory are reported, together with those of the industrial slag used in tests of refractory-slag reactions (reported in the Part 2 paper).

Industrial slag was supplied by an international SiMn producer that produces SiMn using a blend of HCFeMn (high-carbon ferromanganese) slag, manganese ores, quartzite, and coke. At the plant the slag is tapped into ladles and then cast onto slag beds. Once cooled the slag

Table IX. Ratio of Reaction Quotient to Equilibrium Constant (Q/K) at Different Temperatures for Reactions Most Likely to be Responsible for Wear in the Tap Hole; Equilibrium Constants Calculated with FactSage 6.4; Activity Data Used to Calculate the Reaction Quotient, Q, Calculated with FactSage for the Slag Species, and Both FactSage and Li and Morris Interaction Parameters for Metal Species

	1823 K (1550 °C)		1873 K (1600 °C)		1923 K (1650 °C)	
Reaction	FactSage	Li and Morris	FactSage	Li and Morris	FactSage	Li and Morris
$SiO_2 + 3C = SiC + 2CO$	2.4	—	0.9	—	0.3	—
$SiO_2 + 2C = Si + 2CO$	3.3	2.5	1.2	0.8	0.3	0.3
$MnO + C = Mn + CO$	1.2	1.0	0.7	0.6	0.4	0.4

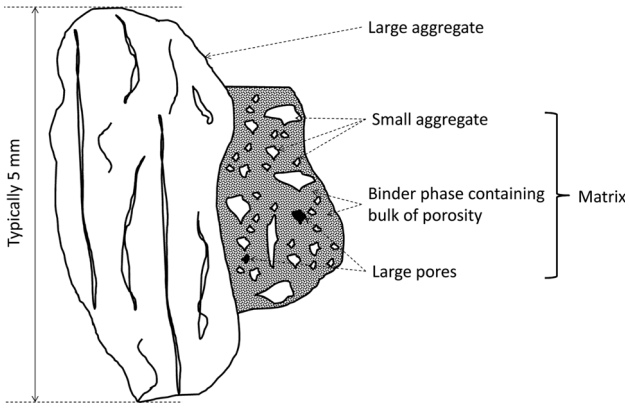

Fig. 3—Schematic drawing of main microstructural features in carbon refractory (carbon block and ramming paste).

is collected by front-end loader. The sample used in the experiments was collected by hand from the slag bed.

The as-received slag was milled with stainless steel balls in a Normand Electrical ball mill, then pulverized in a tungsten carbide sample holder in a swing mill and screened to −425 μm. Using a 10-way rotary splitter, the screened sample was split into subsamples and subsequently into sub–sub samples.

The bulk chemical composition of three representative slag samples was determined by wet chemistry methods; see Table II. Compositions of individual phases were determined by scanning electron microscopy (SEM) with microanalysis by energy-dispersive spectroscopy (EDS), using an acceleration voltage of 15 kV.

Two different types of refractory materials were characterized: carbon block, and cold ramming paste. Both materials consisted of carbon-based aggregate in a matrix consisting of carbon-based binder and small aggregate; see Figure 3 for a diagram of typical microstructural features. Inorganic additives had been added to the binder phase of the carbon block before firing.

A large, unused carbon block sample was received from the project sponsor. No history of the sample was provided. Cold ramming paste samples were supplied by the material supplier both in granular form—as usually supplied to clients as a rammable—and rammed and fired on pilot scale under controlled conditions [inert gas; 1223 K (950 °C)] to simulate plant installation. After firing, samples (50 mm diameter, 50 mm height) were core drilled from the pre-fired ramming paste.

Refractory material samples were analyzed using proximate analysis techniques[15] (similar to coal analysis) to determine the inherent moisture, ash yield, and volatile matter yield, and using ultimate analysis techniques[16] to determine elemental carbon, sulfur, nitrogen, and hydrogen contents (oxygen by difference).

The chemical composition of the ash was determined by inductively coupled plasma (ICP) analysis. As-received materials were submitted for X-ray diffraction (XRD). The type of radiation was copper Kα (copper tube with nickel filter) with the 2θ angle ranging from 5.0084 to 89.9914 degrees and step size 0.0170. The Lc (graphite crystallite size) was calculated from the XRD patterns.[17]

The porosity of three samples each of carbon block, ramming paste aggregate, and ramming paste matrix was determined by X-ray tomography (XRT). For sampling the latter two, one of the pre-baked ramming paste samples was sliced to 3 mm thickness, breaking samples of aggregate and matrix from the slice by hand. XRT was performed at the Nikon XTH 225 ST micro focus system at the MIXRAD facility at the South African Nuclear Energy Corporation (NECSA).[18] Scans were conducted at 100 kV and 100 μA utilizing a tungsten target and a 0.25-mm Cu filter was applied to obtain better transmission, and X-ray characteristics to minimize artifacts. The number of projections was 1000 with an exposure of 25 frames per projection which resulted in scan times of approximately an hour. These scanning parameters resulted in volume elements with linear dimensions of 6.2 to 7.3 μm.

Each dataset was analyzed using VGStudio software associated with the instrument.[18] To calculate the porosity of a material type, pores were identified from differences in gray scale (X-ray absorption) between the air in the pores and the different material types in the sample. The gray-scale intensity associated with a material type was a function of the density of the material.

To estimate pore size distribution, the equivalent pore size (EPS) was defined as the cube root of pore volume. The results were presented as the cumulative pore volume as a function of EPS.

For microscopy of the refractories, polished sections were prepared of the carbon block, the granular ramming paste, and the pre-fired ramming paste, after mounting in epoxy resin with 6 pct iodoform (CHI_3) added to improve atomic number contrast between pores filled with resin and carbon materials in the refractory.[19,20]

B. *Structure and Composition of Industrial Slag and Refractory*

1. *Slag*

Based on microanalysis and X-ray diffraction, the industrial slag consisted primarily of an amorphous slag phase but also contained moissanite (SiC), alabandite (MnS), and intermetallic phases in metal droplets (SiMn, Mn_5Si_3, and Mn_7C_3)—see Figures 4 through 8. A secondary, apparently crystalline slag phase was detected in some of the slag particles (Figure 6; Table X); based on microanalysis and X-ray diffraction, the crystalline phase is probably a pyroxene. Equilib-rium phase compositions of both the amorphous slag

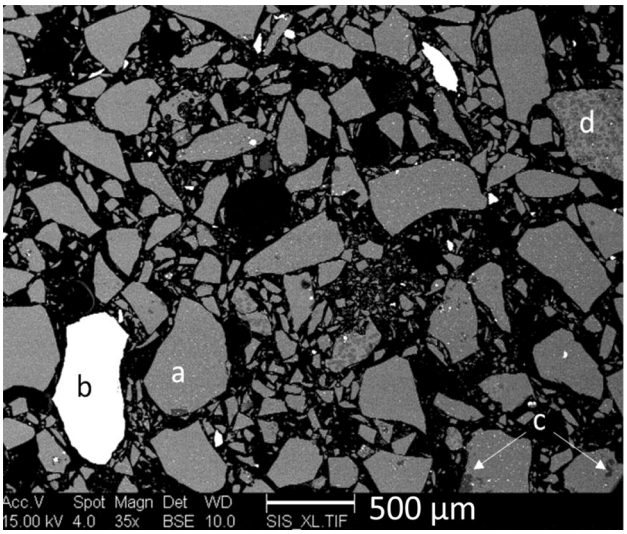

Fig. 4—Backscattered electron micrograph of as-received industrial slag with (*a*) amorphous slag phase containing finely dispersed SiMn metal and MnS droplets, (*b*) large metal particles, (*c*) SiC and (*d*) amorphous slag phase containing secondary slag phase. Scale bar indicates 500 μm.

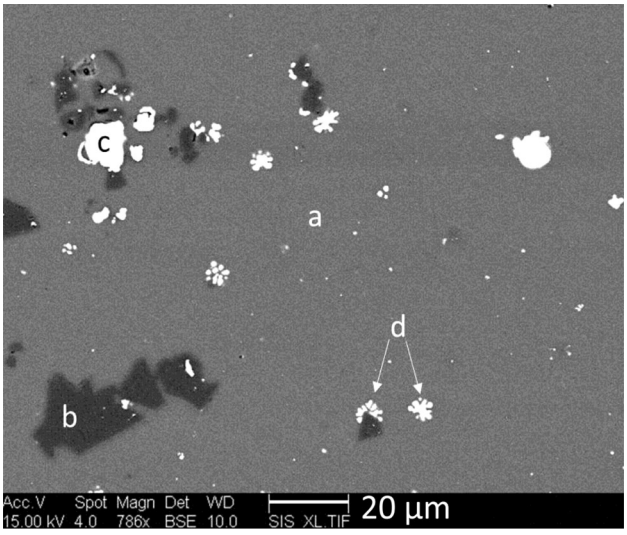

Fig. 5—Backscattered electron micrograph of as-received industrial slag with (*a*) amorphous slag phase, (*b*) SiC phase, (*c*) metal phase and (*d*) MnS. Scale bar indicates 20 μm.

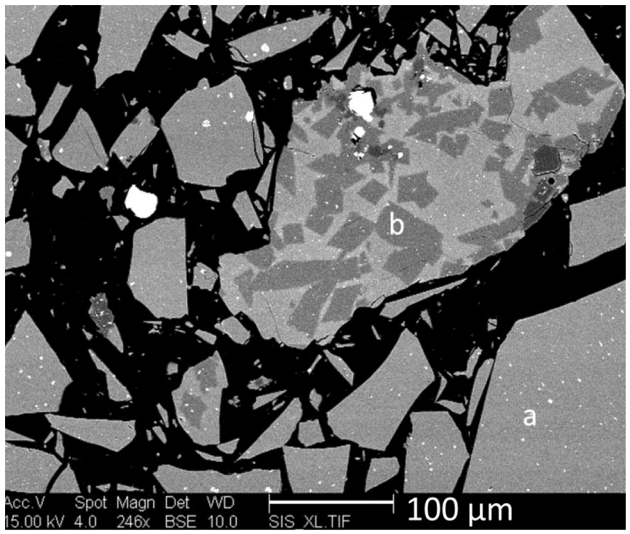

Fig. 6—Backscattered electron micrograph of as-received industrial slag with (*a*) amorphous slag phase and (*b*) secondary slag phase. Scale bar indicates 100 μm.

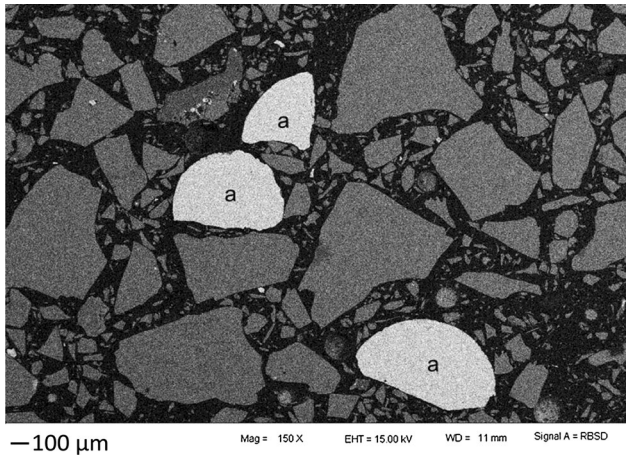

Fig. 7—Backscattered electron micrograph of as-received industrial slag with large metal particles (marked "*a*"). Scale bar indicates 100 μm.

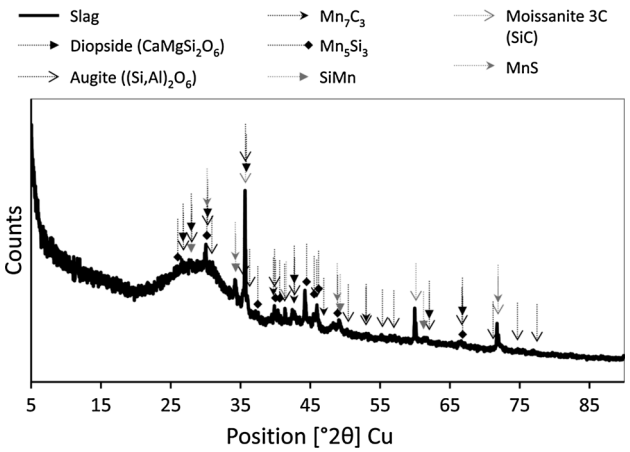

Fig. 8—XRD pattern of the slag sample with markers indicating the main peaks for identified crystalline phases.

Table X. Normalized Elemental Analysis of Slag Phases in the Industrial Slag Sample (Weight Percent; Based on Five EDS Point Analyses Per Phase, Showing Averages and Standard Deviations)

	Na	Mg	Al	Si	S	K	Ca	Mn	Ba	Total
Amorphous slag phase	0.1	7.7	16.5	38.2	0.5	1.1	32.3	2.1	1.6	100.0
SD	0.2	0.2	0.3	0.5	0.1	0.1	0.6	0.3	0.2	
Secondary slag phase	—	11.5	16.8	39.1	—	—	29.8	2.8	—	100.0
SD	—	0.4	1.1	0.9	—	—	0.3	0.7	—	

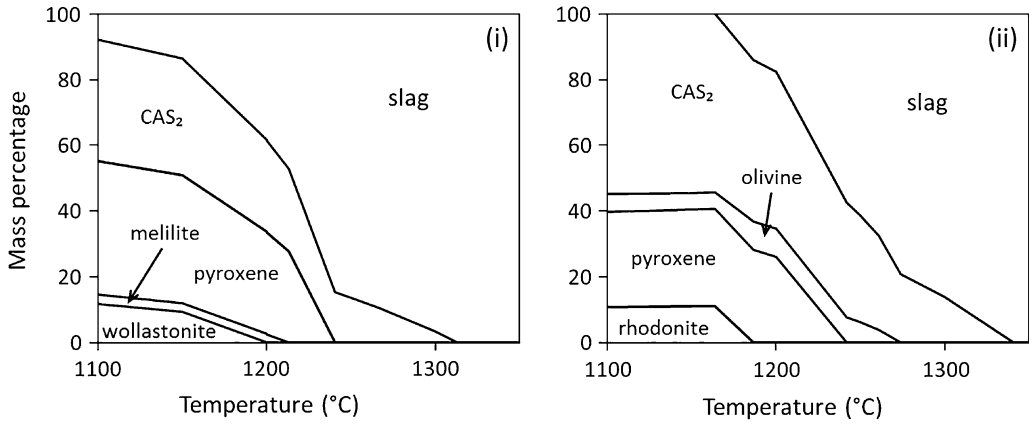

Fig. 9—Equilibrium phase composition (percentage by mass) of (*i*) the amorphous slag phase and (*ii*) the secondary slag phase in the industrial slag sample; calculated with FactSage 6.4.

phase and the secondary slag phase (compositions as in Table X, simplified to Al_2O_3-SiO_2-MgO-MnO-CaO mixtures) were calculated with FactSage (Figure 9); for both compositions, the equilibrium primary phase was anorthite ($CaAl_2Si_2O_8$), followed by pyroxene (and olivine in the case of the secondary slag phase).

According to the equilibrium calculations the slag would be fully liquid in the temperature range 1673 K to 1873 K (1400 °C to 1600 °C); the calculated melting points are below 1623 K (1350 °C). The temperature range 1673 K to 1873 K (1400 °C to 1600 °C) is significant as it was the temperature range over which the laboratory-scale experiments were conducted.

2. *Refractories*

The presence of several species in addition to carbon in both types of refractory is quite evident from the micrographs and X-ray diffraction (Figures 10 through 14). Specifically, phases with higher density (and higher average atomic number) than carbon are evident in the backscattered electron micrographs, and so is the presence of porosity greater than 10 pct. The presence of both non-carbon phases and open porosity is expected to promote slag–carbon reaction by enhancing slag penetration into the refractories.

The proximate analyses (Table XI) confirm the presence of non-carbon species. The ash yield of as-received carbon block was similar to that of micropore brick (20 pct) and significantly higher than that of other carbon bricks (which typically show ≤13 pct ash yield).[21] The ash yield of the ramming paste was typical of carbon refractories.[21] Ash compositions are given in Table XII. In the fired state, the volatile matter yield and moisture contents were similar (and low).

In both types of refractory, carbon was present both as large aggregate particles and in the matrix or binder phase. Based on the width of the "graphite" diffraction peak (Figures 12, 13), the carbon itself was present as mostly amorphous carbon with limited crystallinity. A measure of the degree of crystallinity of carbon is the average thickness of the stacks of aromatic layers (crystallites);[22] this average thickness (L_c) can be calculated from peak broadening in XRD measurements,[17] and results are reported in Table XIII. The crystallite size of carbon in the carbon block was more than twice that of carbon in the ramming paste.

The other crystalline phases identified in the carbon block were moissanite (SiC) and corundum (Al_2O_3). Corundum was present as discrete particles in the matrix and SiC was finely dispersed throughout the matrix (see Figure 11). The SiC had probably been added to the bond matrix to generate microporosity or improve the wear resistance properties of the refractory material.[9,10] Al_2O_3 may have been added for improved resistance to molten metal.[23]

In the pre-fired ramming paste the crystalline phases (other than "graphite") were moissanite (SiC), quartz (SiO_2), cementite (Fe_3C), and mullite ($3Al_2O_3{\cdot}2SiO_2$); these were probably products of calcination of the inorganic materials present in the anthracite.

The porosity measured by XRT is shown in Table - XIV and Figure 14. In Figure 14, round symbols indicate the size of largest pore or series of connected pores (indicative of open porosity) in each sample; full

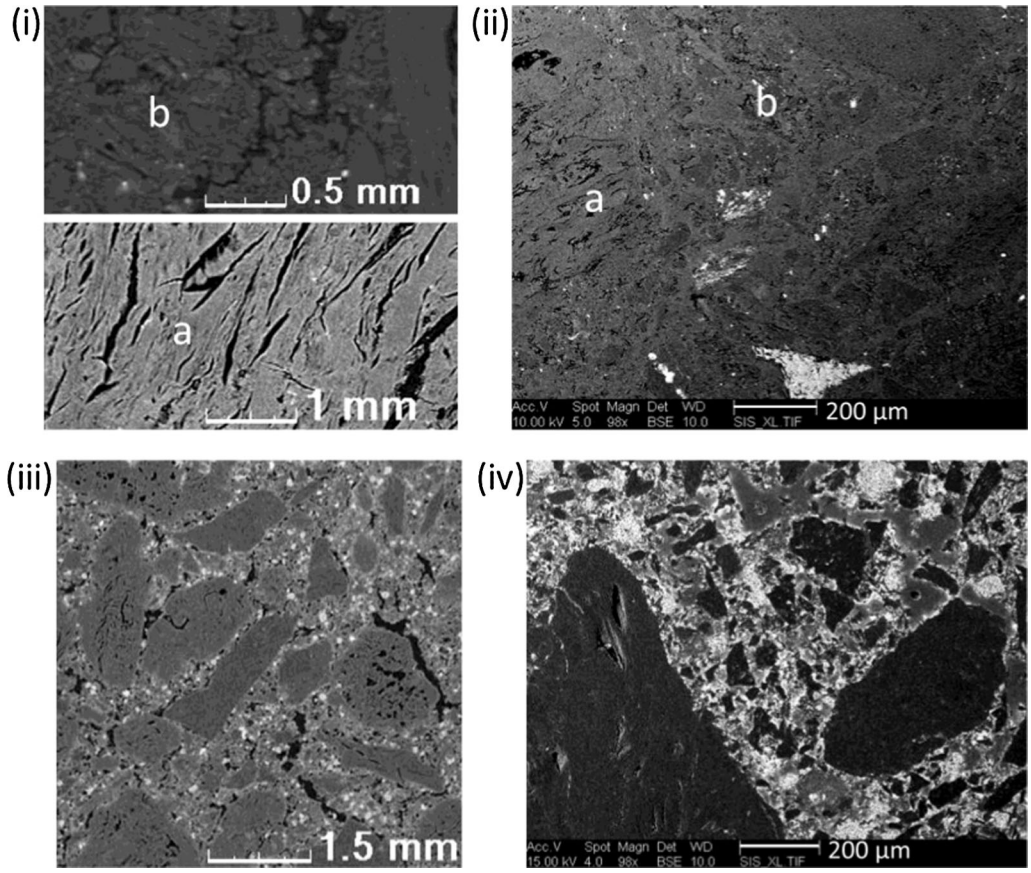

Fig. 10—Micrographs of pre-fired ramming paste: (*i*) XRT images and (*ii*) 10 kV backscattered electron micrograph of (*a*) aggregate and (*b*) matrix; micrographs of carbon block with (*iii*) XRT image and (*iv*) 15 kV backscattered electron micrograph. Scale bar indicates 200 μm in (ii) and 200 μm in (iv).

lines (smaller pores) indicate closed porosity; dashed lines connect data on open pores with the data for closed pores in that XRT sample. Evidently, the porosity of the carbon block was half that of the ramming paste; the porosity of the ramming paste matrix was slightly higher than that of the ramming paste aggregate. For both the carbon block and the ramming paste, open porosity formed a significant part of the total porosity. For carbon block (total porosity approximately 11 pct), 6 to 7 pct of the volume was open and connected porosity—see Figure 14. For ramming paste aggregate (total porosity around 17 pct), 7 to 12 pct of the volume was open porosity, compared with 19 to 21 pct in the ramming paste matrix.

The significant oxide content of the refractories (reflected in the high ash yield) might lead to internal liquid formation in the refractories during use at temperature, even without any slag penetration. To evaluate this possibility, equilibrium phase compositions of the carbon block and the pre-fired ramming paste were calculated with FactSage 6.4. Mass balance calcu-lations based on the fixed carbon and ash yields (Table XI), and ash analyses (Table XII) were used to estimate the chemical composition of the carbon block and pre-fired ramming paste (as input into in the calculations). Although silicon is reported as SiO_2 in the ash analysis, the XRD results show that silicon would be present as SiC in the carbon block (Figure 13) and as a combination of SiC and SiO_2 in the ramming paste (Figure 12). Based on these results the total silicon content was taken to be elemental Si in carbon block, and an equimolar mixture of Si and SiO_2 in ramming paste (Table XV).

Calculations were performed as mentioned earlier, with the difference that calculations converged only if liquid slag were forced to remain a single phase, if present. The results reported are the equilibrium mass percentages of all phases—see Figure 15—over the temperature range considered in experiments.

Metal and slag phases are predicted to form in both refractory materials over the temperature range 1673 K to 1873 K (1400 °C to 1600 °C). In the carbon block—Figure 15(i)—slag and liquid metal are pre-dicted to form upon melting of the spinel, mullite, and anorthite phases present at lower temperatures (with little gas formation). Slag and liquid metal are predicted to form in the ramming paste below 1673 K (1400 °C, Figure 15(ii)). The slag volume is predicted to increase at moderately higher temperatures (by dissolution of cordierite), but decreasing significantly upon the formation of SiC above 1798 K (1525 °C).

Furnace slag would tend to dissolve the solid oxides in the refractories, as shown by Figure 16, which gives the calculated phase compositions for equilibration of equal

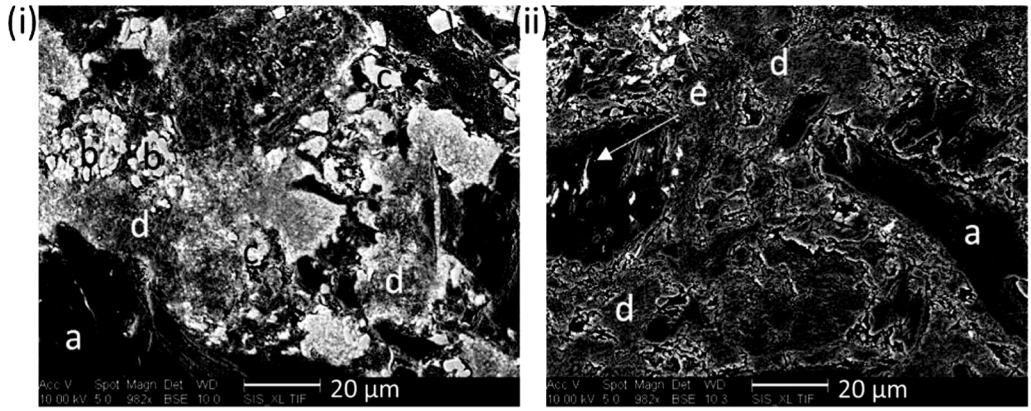

Fig. 11—Higher-magnification backscattered electron micrograph of (*i*) carbon block and (*ii*) pre-fired ramming paste mounted in resin containing 5 pct iodoform showing (*a*) carbon aggregate, (*b*) corundum, (*c*) SiC, (*d*) iodoform-doped resin and (*e*) (Si, Al, K, Na, Fe)-containing minerals. Scale bar indicates 20 μm.

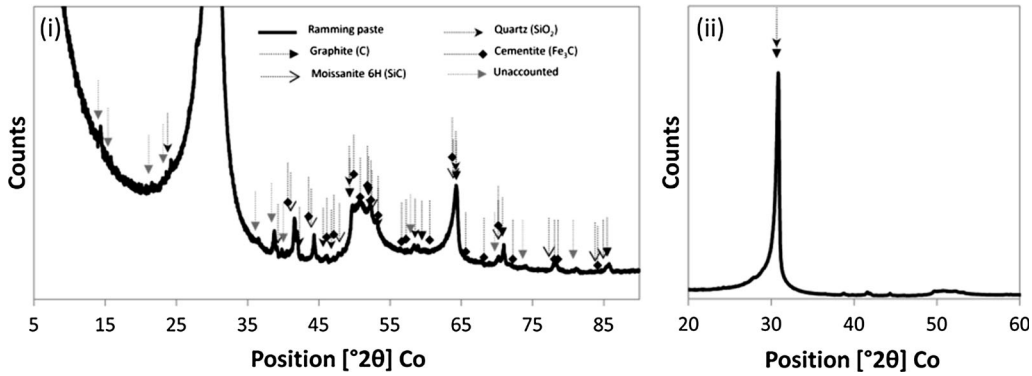

Fig. 12—XRD pattern of the ramming paste refractory sample with markers indicating the significant peaks for phases identified with (*i*) expanded scale to show low intensity peaks and (*ii*) compressed scale to show high intensity peak.

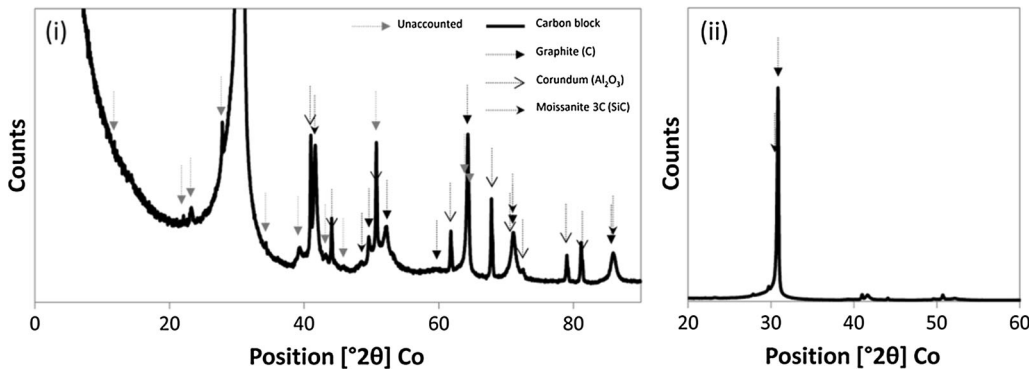

Fig. 13—XRD pattern of the carbon block refractory sample with markers indicating the significant peaks for phases identified with (*i*) expanded scale to show low intensity peaks and (*ii*) compressed scale to show high intensity peak.

masses of slag and pre-baked ramming paste or carbon block (using the industrial slag composition from Table II and refractory compositions in Table XV). For both carbon block and ramming paste, it is predicted that slightly more metal would form (by reduction of MnO) when slag reacted with the refractory material, compared with the amount of metal formed in the absence of slag.

In summary, the analyses of industrial materials (refractories and slag) found pre-existing oxide, silicon carbide, and metal, even before any reaction occured between refractories and slag. For a clearer indication of whether reaction between slag and refractory (producing silicon carbide, or metal, or both) would be possible, tests were performed with purer, synthetic materials, as reported in the next section.

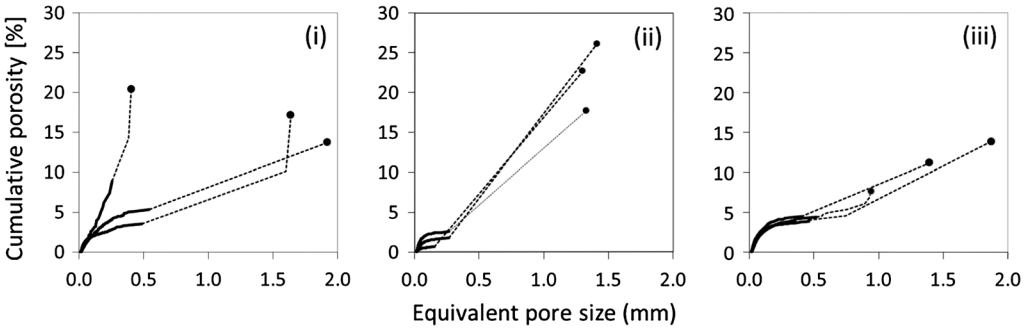

Fig. 14—Pore size distribution measured by XRT for (*i*) ramming paste aggregate, (*ii*) ramming paste matrix and (*iii*) carbon block. Round symbols indicate the size of the largest pore or series of connected pores (open porosity) in a particular sample; full lines (smaller pores) indicate closed porosity; dashed lines connect data on open pores with the data for closed pores in the same XRT sample.

Table XI. Proximate Analyses of the Refractory Materials (Mass Percent)

	Dry Basis			Air-Dried	
	Ash	Volatile	Fixed C	Moisture	Total S
Carbon block	22.7	0.2	77.0	0.1	0.12
Pre-fired ramming paste	6.3	1	92.6	0.1	0.25

Table XII. Bulk Chemical Composition of the Ash Phase Prepared by Combusting the Refractory Material at 1088 K (815 °C) in Air (Mass Percent)

	SiO_2	Al_2O_3	TiO_2	CaO	MgO	FeO	Total
Carbon block	58.2	38.5	0.2	0.4	0.2	2.5	100
Pre-fired ramming paste	56.9	31.3	1.5	1.3	1.2	7.8	100

Table XIII. Crystalite Size (L_c) and Inter Planar Distance (d_{002}) of Carbon in the Refractory Materials

	L_c (Å)	d_{002} (Å)
Carbon block	430	3.4
Pre-fired ramming paste	201	3.4

Table XIV. Total Porosity (Percent) of Refractory Sample Determined by XRT (Three Samples Each, with Average)

	Ramming Paste Matrix 26.1; 17.7; 22.7	Ramming Paste Aggregate 13.7; 20.4; 17.2	Carbon Block 7.6; 11.2; 13.8
Average	22	17	11

Table XV. Chemical Composition (Percentage by Mass) of the Carbon Block and Pre-fired Ramming Paste Used to Calculate the Equilibrium Phase Composition of Both (Based on the Proximate and Ash Analyses in Tables XI and XII, and Si-Bearing Species Identified by XRD)

	C	Si	SiO_2	Al_2O_3	TiO_2	CaO	MgO	FeO	Total
Carbon block	85.55	3.91	—	9.71	0.05	0.10	0.05	0.63	100
Pre-fired ramming paste	94.54	0.86	1.83	2.01	0.10	0.08	0.08	0.50	100

IV. EXPERIMENTAL TEST: REACTION OF SYNTHETIC SLAG WITH PURE CARBON

A. *Experimental Approach*

Pure graphite crucibles were exposed to a synthetic, five-component slag at 1823 K or 1923 K (1550 °C or 1650 °C), under argon. Based on previous experi-ments —some conducted by Mølna˚s[7]—4 hours was selected as a suitable duration.

Synthetic slag was prepared mixing pure oxides, homogenizing the mixture (by splitting into ten subsamples using a 3-way splitter, and recombining the

Table XVI. Analysis (Mass Percent) of Metal Accumulated at the Slag/Refractory Interface After Reaction at 1823 K and 1923 K (1550 °C and 1650 °C), Measured by EDS Point Analysis at 15 kV (Averages, with Standard Deviation in Parenthesis)

	Si	Mn	Fe	Cr	Ni
1823 K (1550 °C)	15.6 (5.7)	63.1 (6.3)	17.4 (0.3)	2.5 (0.4)	1.4 (0.7)
1923 K (1650 °C)	20.2 (4.5)	71.4 (5)	6.8 (0.6)	1.1 (0.1)	0.7 (0.2)

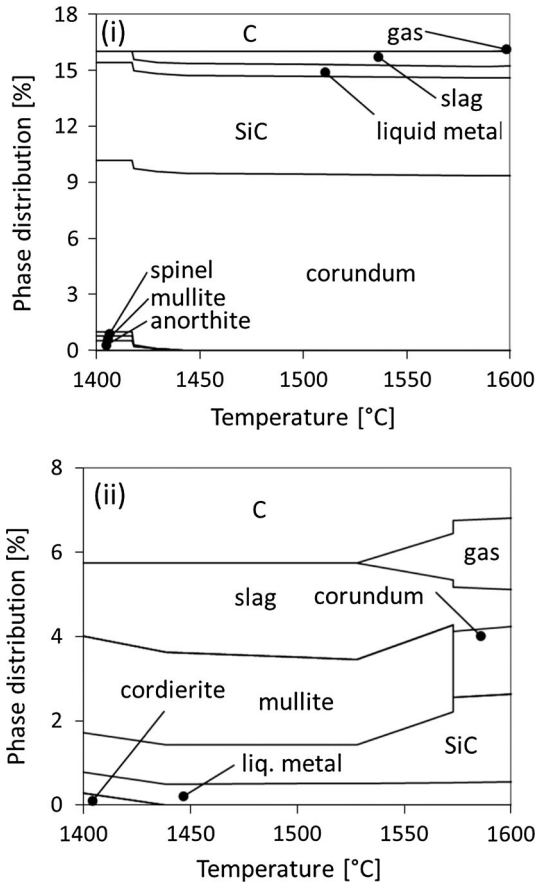

Fig. 15—Equilibrium phase composition (percentage by mass) of (*i*) the carbon block and (*ii*) the pre-fired ramming paste based on the chemical compositions in Table XV; calculated with FactSage 6.4.

subsamples into one sample; repeated three times), and melted in a 50 kg-capacity induction furnace (with a custom-made graphite crucible serving as susceptor). During melting, a protective atmosphere was created by covering the crucible with a mineral wool blanket and blowing argon through a pipe with the outlet placed below the surface.

As mentioned earlier, the predicted liquidus temperature of the ''typical'' slag listed in Table II is approximately 1508 K (1235 °C). For slag melting, the target temperature was taken to be 100 K (100 °C) above the melting point, controlling temperature by manually changing the power input to the furnace. Temperature was measured with a type R thermocouple (protected by both an alumina and a graphite sheath) placed below the slag surface. After melting, the slag was poured into a graphite slag pot and allowed to solidify and cool.

Once cooled, the slag was manually broken out of the slag pot using a hammer and chisel. The crushed slag was milled with stainless steel balls in a Normand Electrical ball mill, pulverized in a tungsten carbide sample holder in a swing mill and screened to −425 μm. The screened sample was split into subsamples and subsequently into sub–sub samples using a 10-way rotary splitter.

One of the representative, sub–sub samples of slag was characterized as follows:

1. Bulk chemical composition was determined by wet chemical methods at an in-house laboratory at a South African producer of SiMn with ISO 9001:2000 accreditation:

- Inductively coupled plasma (ICP): FeO, CaO, MgO, Al_2O_3
- Gravimetry: SiO_2
- Titration: MnO

2. Bulk phases were determined by X-ray diffraction (XRD).
3. Compositions of specific phases were determined by:

- Preparing polished sections and sputter coating these with gold
- Microanalysis within a scanning electron microscope, using energy-dispersive spectroscopy (EDS) at 15 kV (point analyses)

The measured composition of the prepared (melted and ground) synthetic slag (Table II) was found to be close to the targeted typical slag composition. The calculated equilibrium phase composition of this slag (calculated with FactSage, using the same approach mentioned earlier) indicated that the slag would be fully molten at the test temperatures of 1823 K and 1923 K (1550 °C and 1650 °C) (Figure 17). The lack of back-scattered electron contrast within the solidified slag (Figure 17) indicated it to be amorphous, and this was confirmed by XRD. EDS microanalysis yielded similar mass percentages to wet chemical analysis (Table II).

A schematic of the experimental setup for reaction of the prepared synthetic slag with pure graphite is given in Figure 18. In each experiment a small graphite crucible (9 mm inner diameter, 45 mm height) was filled with a 5 g representative synthetic slag sample. The crucible was placed in a graphite susceptor with graphite lid supported by bubble alumina (J). The graphite lid (G) had two 10 mm ports—inlets for the alumina thermocouple sheath (C) and alumina sleeve (D) used to blow 99.998 pct argon gas onto the surface of the lid—and five 6 mm ventilation holes (F) for gasses to escape. The induction coil was cast in coil grout (I).The graphite susceptor was supported by bubble alumina. The top of

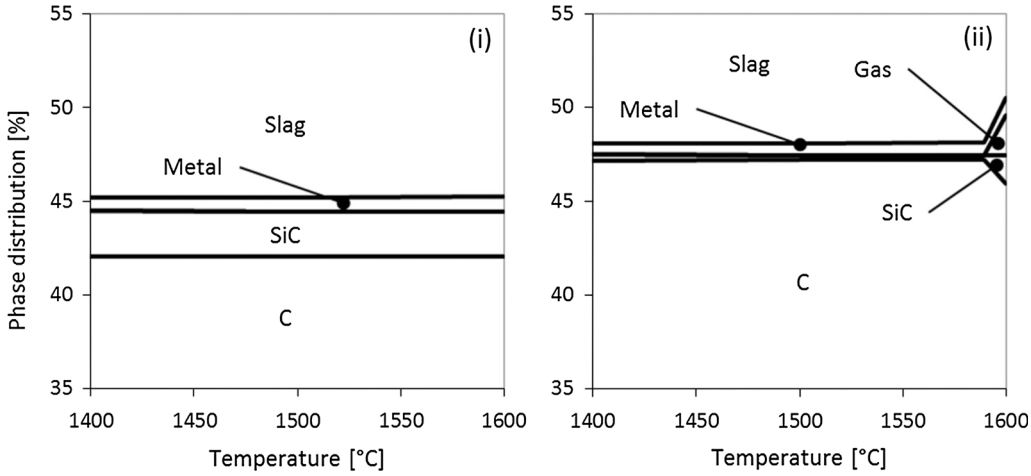

Fig. 16—Equilibrium phase composition when reacting industrial slag with an equal mass of (*i*) carbon block and (*ii*) pre-baked ramming paste. (Slag composition as given in Table II and refractory compositions as in Table XV).

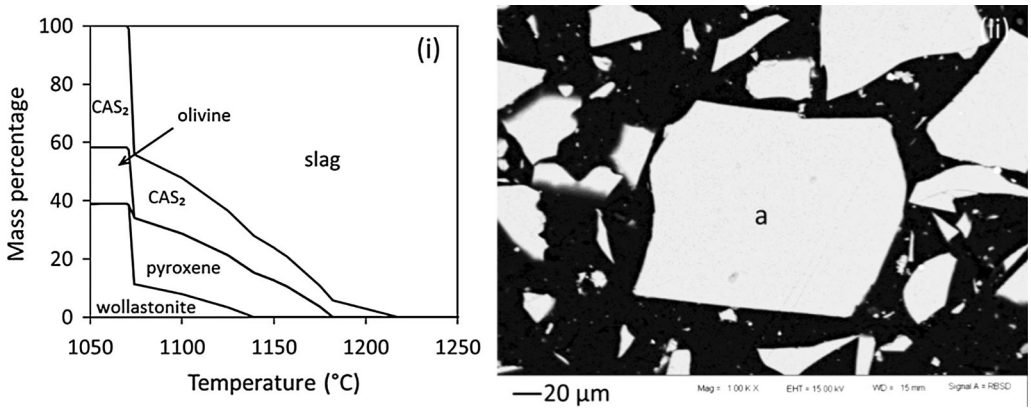

Fig. 17—(*i*) Equilibrium phase composition of synthetic slag based on the bulk chemical composition, as calculated with FactSage 6.4. (*ii*) Backscattered electron image of synthetic slag (scale bar 20 μm) with (*a*) amorphous slag phase only.

the graphite susceptor was aligned with the top of the induction coil grout.

Energy was supplied by an Ambrell Ecoheat ES high-frequency induction furnace. Temperature was measured with type B and R thermocouples wired through a four-bore alumina sleeve (M) allowing the hot junctions to be positioned at the same level. The type B thermocouple was used as the control temperature with readings logged manually. The type R thermocouple was used as the reference thermocouple with temperature readings logged automatically. The temperature was controlled by manually changing the voltage set point on the induction furnace control panel.

To control the atmosphere, the experimental setup was contained in a stainless steel shell—L—with stainless steel lid. The lid had inlet ports for the thermocouple sheath and argon supply and an outlet port for the off gasses (A). Joints were sealed using gaskets cut from high temperature silicone and high temperature O-rings.

To improve thermal insulation a precast refractory cylinder—K—and refractory lid were positioned in the steel shell. The gaps between the steel shell and refractory cylinder, and between the refractory cylinder and induction coil were filled with bubble alumina. The susceptor lid was covered by three layers of 30 mm thick, high temperature refractory blanket—E—(Rath Altra Mat 80) with openings for the thermocouple sheath and argon sleeve.

When the experimental setup was assembled, the chamber was flushed with argon. After 20 minutes of flushing, the power was switched on and the sample was heated to 1823 K or 1923 K (1550 °C or 1650 °C) by manually adjusting the target voltage set point. The temperature was held for 4 hours by manually adjusting the voltage set point when required. During the holding period the control temperature readings ranged ±5 °C around the set point. After 4 hours at the holding temperature, the power was switched off, argon flow was stopped, and the furnace opened immediately to cool the sample rapidly. The sample was removed from the furnace the next morning and mounted in epoxy for polishing of cross sections.

V. RESULTS AND DISCUSSION

Backscattered electron micrographs (Figures 19, 20) showed the presence of metal at the slag/carbon interface after reactions at both 1823 K and 1923 K

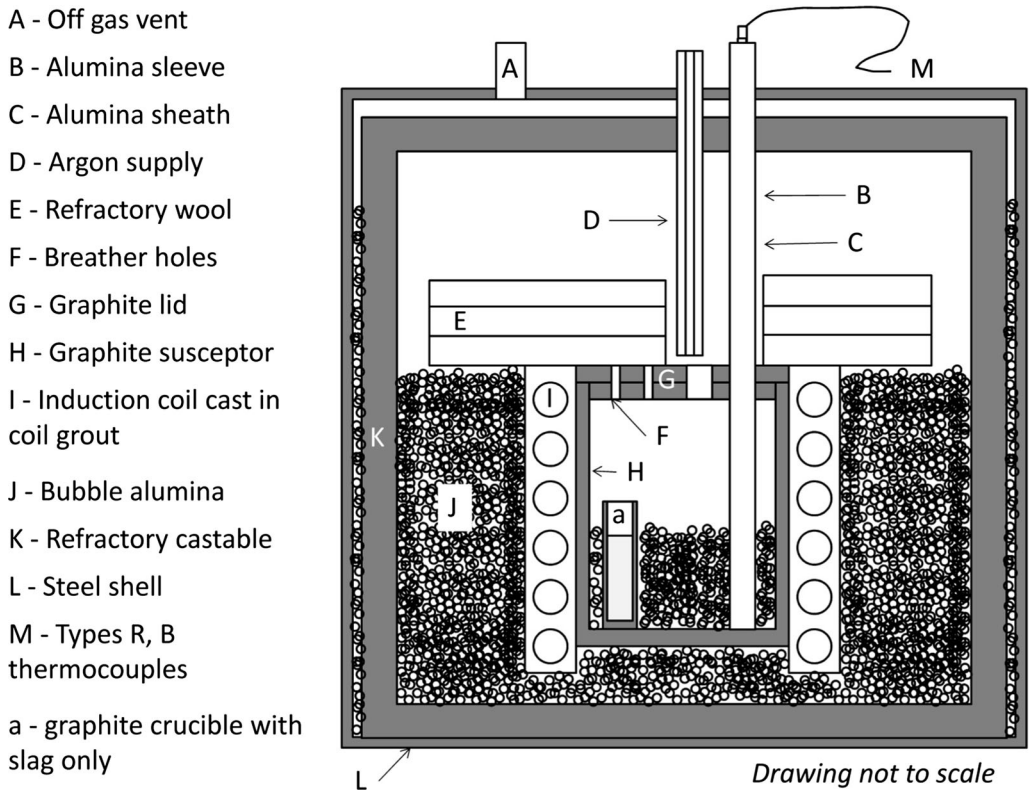

Fig. 18—Experimental setup for pure component experiments.

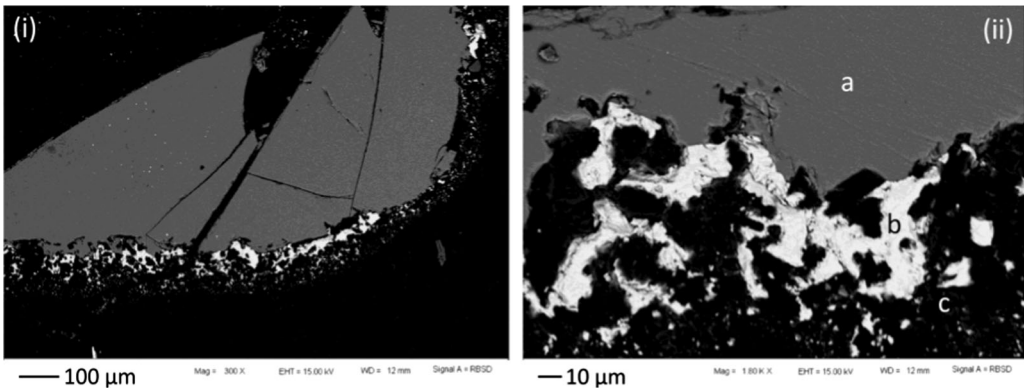

Fig. 19—Backscattered electron micrographs of metal accumulation at the slag/carbon interface after reaction at 1823 K (1550 °C), showing (*i*) lower magnification (scale bar 100 μm) and (*ii*) higher magnification (scale bar 10 μm); phases are (*a*) slag, (*b*) metal and (*c*) graphite.

(1550 °C and 1650 °C). Microanalysis of the metal (Table XVI) showed, in addition to Si and Mn, the unexpected presence of Fe, Cr, and Ni contamination, most probably originating from the balls used to mill the slag.

The effect of metallic contamination on the potential for slag–carbon reactions was estimated with FactSage. Relative masses of slag, carbon, and steel contaminant used in the calculations were 100:100:(0.5 or 5.0). The composition of the steel contaminant used in the calculations is given in Table XVII (estimated from metal analyses in Table XVI, assuming all of the Fe, Cr, and Ni to have originated from the contamination, and none of the Si and Mn). The results in Figure 21 show that the presence of steel contaminant would have allowed minor reduction (to metal) of MnO and SiO_2 to occur at temperatures lower than 1823 K (1450 °C) (as indicated by an increase in metal mass and gas formation). The effect of contamination on silicon carbide formation was predicted to be insignificant (as would be expected, since the metallic phase is not involved directly in formation of silicon carbide).

Electron microscopy showed that SiC did form in the experiments at the higher temperature 1923 K (1650 °C)

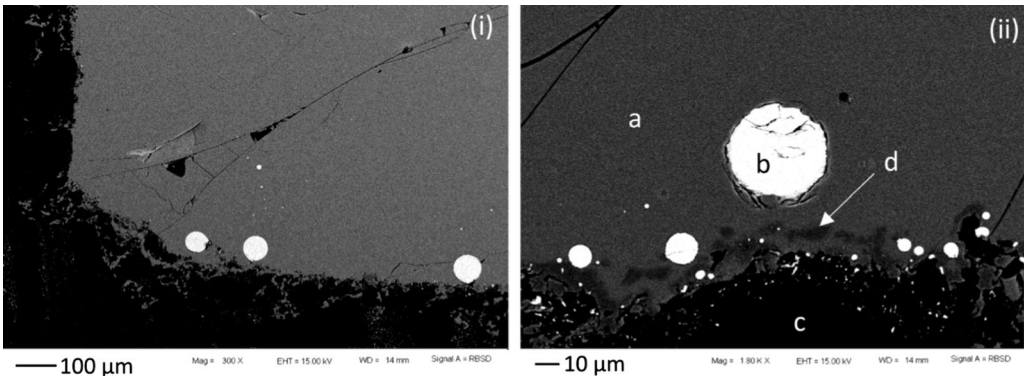

Fig. 20—Backscattered electron micrographs of metal accumulation at the slag/carbon interface after reaction at 1923 K (1650 °C), showing (*i*) lower magnification (scale bar 100 μm) and (*ii*) higher magnification (scale bar 10 μm); phases present were (*a*) slag, (*b*) metal, (*c*) graphite and (*d*) SiC. Note that the SiC did not form a protective layer at the slag/refractory interface, but detached from the graphite.

Table XVII. Estimated Composition of Steel Contaminant (Mass Percent)

Si	Mn	Fe	Cr	Ni
0	0	81.7	11.7	6.6

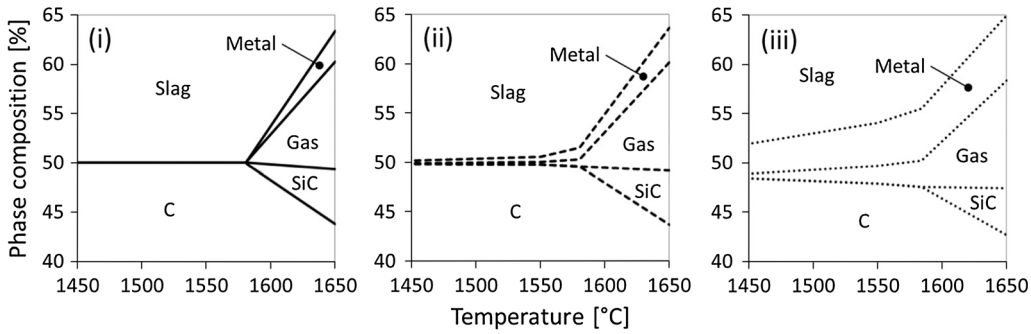

Fig. 21—Equilibrium phase composition for equilibration of synthetic slag with an equal mass of graphite, for cases with (*i*) no steel contaminant, (*ii*) 0.5 g steel contaminant per 100 g slag added and (*iii*) 5.0 g steel contaminant per 100 g slag. Calculated with FactSage.

but not at the lower temperature 1823 K (1550 °C), in line with thermodynamic predictions (see Figures 19, 20, 21), and confirming the possibility of chemical wear of carbon refractory by formation of silicon carbide. The SiC did not form as a continuous layer at the slag/carbon interface, but detached from the interface. This observation suggests that silicon carbide formation would not serve to protect the carbon refractory from further reaction. Some of the SiC particles were observed to be attached to metal droplets.

VI. CONCLUSIONS

Thermodynamic calculations suggest that reaction between silicomanganese slag and carbon-based tap-hole refractory is possible, and experiments with nominally pure materials support this. In the experiments the SiC reaction product that formed, detached from the graphite surface. This implies that chemical reaction between carbon-based refractory in the tap hole and silicomanganese slag and metal is a potential wear mechanism. However, practical refractory materials are by no means pure materials, and contain secondary phases and porosity which can be expected to affect reaction with slag. Such reactions are examined in Part 2.

ACKNOWLEDGMENTS

We are grateful for guidance on the research topic and funding provided by the anonymous industrial project sponsor, and for additional funding by the National Research Foundation of South Africa (Grant TP2011070800005).

REFERENCES

1. S.E. Olsen, M. Tangstad, and T. Lindstad: *Production of Manganese Ferroalloys*, Tapir Academic Press, Trondheim, Norway, 2007, pp. 1–247.
2. S.E. Olsen and M. Tangstad: in *INFACON X: Transformation Through Technology*, South African Institute of Mining and Metallurgy, Cape Town, South Africa, 2004, pp. 231–38.
3. F. Habashi: *Handbook of Extractive Metallurgy*, vol. 1, Wiley-VCH, Weinheim, 1997.
4. D.B. Wellbeloved, P.M. Craven, and J.W. Waudby: in *Ullmann's Encyclopedia of Industrial Chemistry*, Wiley-VCH, Weinheim, 2012, pp. 175–221.
5. J.D. Steenkamp, J.P. Gous, P.C. Pistorius, M. Tangstad, and J.H. Zietsman: in *Furnace Tapping Conference 2014*, Southern African Institute of Mining and Metallurgy, Johannesburg, South Africa, 2014, pp. 51–64.
6. J. Steenkamp, M. Tangstad, P. Pistorius, H. Mølnås, and J. Muller: in *INFACON XIII*, P. Dipner, Almaty, Kazakhstan, 2013, pp. 669–76.
7. H. Mølnås: Master's Degree Thesis, Norwegian University of Science and Technology, 2011.
8. A.M. Hearn, A.J. Dzermejko, and P.H. Lamont: in *8th International Ferroalloys Congress*, China Science & Technology Press, Beijing, China, 1998, pp. 401–26.
9. J. Tomala and S. Basista: in *Infacon XI: Innovation in Ferroalloy Industry*, Indian Ferroalloy Producers Association, New Delhi, India, 2007, pp. 722–27.
10. K. Piel and A. Schnittker: in *Handbook of Refractory Materials: Design|Properties|Testings*, 4th ed., Vulkan-Verlag Essen, 2012, pp. 48–51.
11. F. Prins: Personal communication: Elkem carbon ramming pastes, 2011.
12. H. Brun: *J. Inst. Refract. Eng.*, 1982, no. Spring, pp. 12–23.
13. C. Bale, P. Chartrand, S. Degterov, and G. Eriksson: *CALPHAD*, 2002, vol. 26, pp. 189–228.
14. H. Li and A. Morris: *Metall. Mater. Trans. B*, 1997, vol. 28B, pp. 553–62.
15. ASTM Standards D3172-07a: *Proximate Analysis of Coal and Coke*, ASTM International, West Conshohocken, PA, 2003, pp. 1–2, 2007.
16. ASTM Standards D3176-09: *Ultimate Analysis of Coal and Coke*, ASTM International, West Conshohocken, PA, 2003, pp. 1–4, 2009.
17. ASTM Standards D5187-10: *Annual Book of ASTM Standards*, no. C. ASTM International, West Conshohocken, PA, 2003, pp. 1–4, 2010.
18. J.W. Hoffman and F.C. De Beer: in *18th World Conference on Nondestructive Testing*, South African Institute for Non-Destructive Testing, Durban, South Africa, 2012.
19. C.O. Gomez, D.W. Strickler, and L.G. Austin: *J. Electron Microsc. Tech.*, 1984, vol. 1, pp. 285–87.
20. W.E. Straszheim, K.A. Younkin, R.T. Greer, and R. Markuszewski: *Scanning Microsc.*, 1988, vol. 2 (3), pp. 1257–64.
21. A.J. Dzermejko: in *Refractories Handbook*, 1st ed., C. Schacht, ed., CRC Press, Boca Raton, 2004, pp. 217–30.
22. P.C. Pistorius: *J. South. Afr. Inst. Min. Metall.*, 2002, vol. 102, pp. 33–36.
23. M. Nitta: *Nippon Steel Tech. Rep.*, 2006, vol. 94 (July), pp. 122–26.